Surface Chemistry

DOI: 10.1002/anie.200604399

F Centers versus Dimer Vacancies on ZnO Surfaces: Characterization by STM and STS Calculations**

Roman Kováčik, Bernd Meyer, and Dominik Marx*

Perfectly ordered oxide surfaces are usually quite inert, so that their chemical reactivity and catalytic properties are commonly attributed to the presence of surface defects.[1] Oxygen vacancies, also called *F* centers, are traditionally considered to be both the most abundant and the chemically most reactive type of atomic surface defect for a large variety of oxides.[2] For example, the dissociation of water on TiO_2(110) has been shown to be activated by O vacancies,[3,4] and *F* centers on metal oxide supports, in particular MgO(001), are held responsible for anchoring deposited metal nanoclusters and for controlling their charge state, thereby promoting the activation of adsorbed reactant molecules.[5,6] However, in a recent combined scanning tunneling microscopy (STM) and electron paramagnetic resonance (EPR) study of the MgO(001) surface, a significant concentration of such *F* centers could be observed only after electron bombardment.[7] In electronic-structure calculations studying the chemical reactivity of *F* centers (typically carried out at zero temperature and pressure), the O vacancies are postulated to exist,[4–6] but detailed investigations as to whether they are actually the thermodynamically most favorable type of surface defect under the ambient conditions of relevant chemical processes are lacking.

Experimentally, O vacancies are difficult to observe with most spectroscopic surface science techniques, since their concentration is usually low. Thus, STM as a local real-space probe has become a preferred tool for identifying and characterizing atomic surface defects. STM has been used successfully, for example, to image O vacancies on various metal oxides, such as NiO(001),[8] CeO_2(111),[9] or MgO(001).[7,10] A further advantage of STM is that it can be applied to as-grown material, to nanoparticles, and also in situ under realistic conditions where surface chemical processes are carried out.

[*] Dipl.-Phys. R. Kováčik, Dr. B. Meyer, Prof. Dr. D. Marx
Lehrstuhl für Theoretische Chemie
Ruhr-Universität Bochum
44780 Bochum (Germany)
Fax: (+49) 234-32-14045
E-mail: bernd.meyer@theochem.rub.de

[**] We thank U. Diebold, U. Köhler, A. Birkner, and C. Wöll for stimulating discussions of STM/STS experiments. This work was supported by the German Research Foundation (DFG) within the framework of the Collaborative Research Center SFB 558 "Metal–Substrate Interactions in Heterogeneous Catalysis". R.K. acknowledges financial support through his Kekulé Fellowship from the Fonds der Chemischen Industrie (FCI). Computational resources were provided by HLRS (Stuttgart), BOVILAB@RUB (Bochum), and Resourcenverbund NRW.

In this Communication, we systematically investigate the thermodynamics of different atomic defects on the nonpolar ZnO(10$\bar{1}$0) surface, and we calculate the associated STM images and spectra from scanning tunneling spectroscopy (STS). The advantage of ZnO is that it has been very well characterized in recent years owing to its importance in various fields, such as semiconductor device technology and heterogeneous catalysis.[11,12] This attention has given rise to several surprising findings, especially for the nonpolar ZnO-(10$\bar{1}$0) surface, such as surface metallization upon hydrogen adsorption[13] and partial dissociation of water layers on defect-free surfaces.[14] It will be shown that not *F* centers but missing ZnO dimers are the most characteristic atomic defects on the ZnO(10$\bar{1}$0) surface, not only in typical ultra-high vacuum (UHV) experiments but also at catalytic (T,p) conditions. This result convincingly explains recent experimental findings of the different catalytic activities and properties between the polar and nonpolar ZnO terminations, as discussed in the outlook below. The most direct evidence to support this view should come from STM-based experiments. To this end, the pertinent defect types are analyzed and found to yield characteristic differences in their STM images and STS spectra, which should serve as fingerprints for an identification of these various defects in future experiments.

ZnO crystallizes in the hexagonal wurtzite structure. Its nonpolar ZnO(10$\bar{1}$0) surface is characterized by ZnO surface dimer rows along the [1$\bar{2}$10] direction, which are separated by trenches.[15] Its most simple atomic defects are O vacancies (O-v), Zn vacancies (Zn-v), and the removal of complete ZnO dimers (ZnO-v). In order to calculate the vacancy formation energies E_v as a function of the redox properties of a surrounding gas phase,[16] chemical potentials μ_O and μ_{Zn} are introduced, which represent the energies of the reservoirs with which the O and Zn atoms are exchanged when a defect is created or annihilated.[17] Assuming that the surface is in thermodynamic equilibrium with the underlying bulk material, the chemical potentials have to fulfill $\mu_O + \mu_{Zn} = E_{bulk}^{ZnO}$, where E_{bulk}^{ZnO} is the energy of one ZnO bulk unit cell. Upper limits for μ_O and μ_{Zn} are given by the total energies of their most stable elemental phases, that is, molecular oxygen $\frac{1}{2}E_{mol}^{O_2}$ and metallic zinc E_{bulk}^{Zn}. If the chemical potentials were to exceed these limits, the surface energy could be lowered by simply precipitating the elemental phases.[17] Using both relations, μ_{Zn} can be eliminated, and simultaneously a lower bound for μ_O is introduced. Taking the upper bound of μ_O as a new zero point of energy by introducing $\Delta\mu_O = \mu_O - \frac{1}{2}E_{mol}^{O_2}$, the allowed range for $\Delta\mu_O$ is $-E_{form}^{ZnO} \le \Delta\mu_O \le 0$, where $E_{form}^{ZnO} = E_{bulk}^{Zn} + \frac{1}{2}E_{mol}^{O_2} - E_{bulk}^{ZnO}$ is the formation energy of bulk ZnO from metallic zinc and molecular oxygen, for which the

experimental value of 3.6 eV has been used.[18] The vacancy formation energies E_v are then given by Equations (1)[16]

$$\begin{aligned} E_v^O &= E_{slab}^{O\text{-}v} + \mu_O - E_{slab}^{ideal} = E_{slab}^{O\text{-}v} + \frac{1}{2}E_{mol}^{O_2} - E_{slab}^{ideal} + \Delta\mu_O \\ E_v^{Zn} &= E_{slab}^{Zn\text{-}v} + \mu_{Zn} - E_{slab}^{ideal} = E_{slab}^{Zn\text{-}v} + E_{bulk}^{ZnO} - \frac{1}{2}E_{mol}^{O_2} - E_{slab}^{ideal} - \Delta\mu_O \\ E_v^{ZnO} &= E_{slab}^{ZnO\text{-}v} + \mu_O + \mu_{Zn} - E_{slab}^{ideal} = E_{slab}^{ZnO\text{-}v} + E_{bulk}^{ZnO} - E_{slab}^{ideal}, \end{aligned} \quad (1)$$

where E_{slab} are the total energies of ZnO slabs with and without defect. All required total energies were calculated by applying density functional theory using the CPMD package.[19] The gradient-corrected PBE functional has been used together with Vanderbilt ultrasoft pseudopotentials and plane waves up to a cut-off energy of 25 Ry; k-point sampling was restricted to the Γ point, and the upper half of the periodically repeated slabs was fully relaxed. Characteristic relaxations of neighboring atoms next to the defects, which have a significant influence on the topography of the STM images, are described below.

The defect formation energies are found to be converged for a slab thickness of eight atomic layers and a lateral extension of (4×2) surface unit cells, as demonstrated by the data compiled in Table 1. The converged defect formation energies are plotted as function of $\Delta\mu_O$ in Figure 1a. A phase diagram of the (T,p) conditions at which each of the three vacancies is the most stable atomic defect type was obtained by converting μ_O into temperature and oxygen partial pressure following reference [20]. Figure 1b reveals that under almost all experimentally relevant (T,p) conditions, ZnO-dimer vacancies have the lowest formation energy and will therefore be the most abundant type of atomic defect. Only in a strongly oxidizing environment do isolated Zn vacancies become lower in energy, and very reducing conditions are needed for isolated O vacancies to be the most favorable atomic defects (Figure 1a). The reason for this strong preference for ZnO-dimer vacancies is that their formation energy amounts to only 1.0 eV, whereas for the creation of a separated Zn and O vacancy pair an energy of 3.6 eV is required. Thus, at standard UHV as well as at typical industrial catalysis conditions as sketched in Figure 1b, it is found that basically no O vacancies should be present. If created, they are expected to readily convert into ZnO-dimer vacancies by desorption of Zn atoms or to be removed by O atoms from the bulk or by traces of oxygen in the gas phase.

Table 1: Formation energies [in eV] of O, Zn, and ZnO-dimer vacancies on the nonpolar ZnO$(10\bar{1}0)$ surface.[a]

Unit cell	N_L	N_{at}	$E_v^O-\Delta\mu_O$	$E_v^{Zn}+\Delta\mu_O$	E_v^{ZnO}
(3×2)	4	48	2.87	0.62	1.49
	6	72	2.90	0.40	1.06
	8	96	2.91	0.45	0.97
	10	120	2.91	0.41	0.95
(4×2)	6	96	3.05	0.50	1.07
	8	128	3.05	0.53	0.97
	10	160	3.05	0.47	0.95
(5×3)	8	240	3.17	0.51	1.03

[a] As a function of the surface unit cell size $(n\times m)$ and the slab thickness N_L, yielding N_{at} atoms in the supercell calculation.

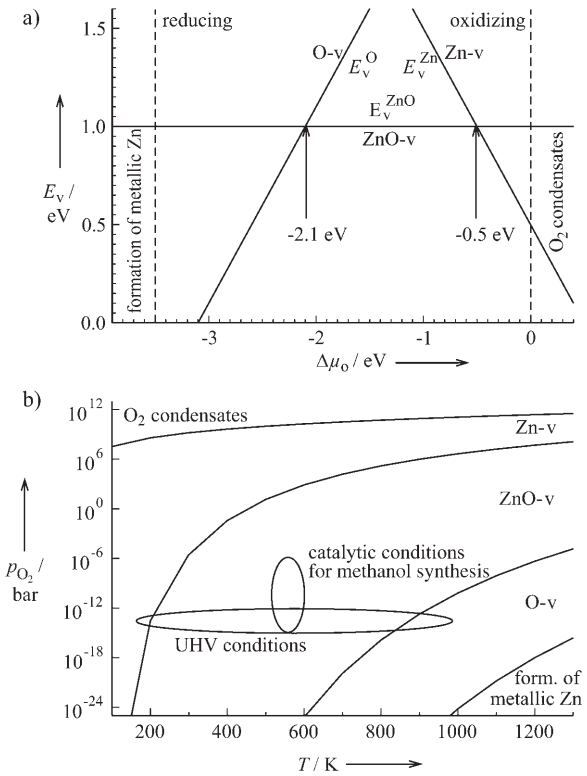

Figure 1. a) Formation energy of different atomic defects on the ZnO-$(10\bar{1}0)$ surface as a function of the oxygen chemical potential $\Delta\mu_O$ of a surrounding gas phase. b) Phase diagram of the most abundant atomic defects after the chemical potential has been converted into temperature and pressure conditions using thermochemical data.

Having found that F centers are basically absent at experimentally relevant conditions, we expect the ZnO$(10\bar{1}0)$ surface to show a vastly different behavior than what is commonly discussed for metal oxide surfaces. To provide guidelines which allow an experimental verification that indeed ZnO-dimer vacancies and not F centers prevail at the ZnO$(10\bar{1}0)$ surface, STM images and STS spectra for the different atomic defects have been calculated using our implementation of the Bardeen tunneling formula[21] into the CPMD code.[19] In the Bardeen approach, the local electronic structure of the surface and of the tip are taken into account explicitly, which allows systematic studies of the influence of tip modifications on the STM data (e.g. contrast inversion caused by adatoms at the tip apex). Large (5×3) surface unit cells and seven different tungsten tips with different shapes and orientations were used to calculate STM images and STS spectra.[22] The tips were modeled by small pyramids supported on a W slab with either (100), (110), or (111) orientation. Furthermore, H and O impurities attached to or in place of the apex W atom were considered, as depicted in Figure 2.

Even at first glance, very characteristic differences between the STM images and STS spectra of the various defects are evident in Figure 2. The ZnO valence and conduction bands are mainly formed by O 2p and Zn 4s

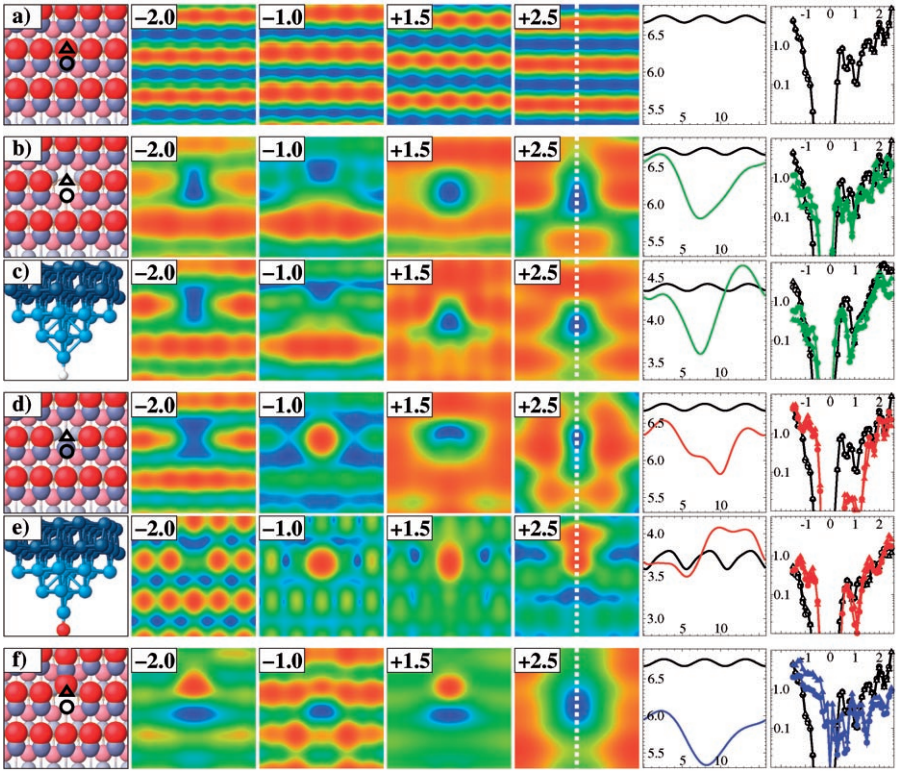

Figure 2. STM images of the ZnO(10$\bar{1}$0) surface ((5×3) surface unit cells, corresponding to 16×16 Å^2) for different bias voltages (in V, given as labels in columns 2–5) and a constant tunneling current of 10 nA: a) ideal termination; b,c) ZnO-dimer vacancy; d,e) O vacancy; f) Zn vacancy. The surface–tip distance is color-coded (blue/red—minimum/maximum distance). In (a,b,d,f), a (110)-oriented pure W tip was used, and column 1 displays top views of the corresponding relaxed surface structures. In (c) and (e), tip models with an adsorbed H and O atom, respectively, were employed, shown in column 1 instead of the underlying surface structure: Zn gray, O red, H white, W blue. The position of line scans (shown in column 6, surface–tip distance and lateral position in Å) is marked by a dashed white line. STS *I*(*V*) curves are displayed in the last column (current in nA, voltage in V). The spectra are taken for a tip–surface distance of 7 Å (a,b,d,f) and 5 Å (c,e) above the position of the Zn atom and the O atom of the central ZnO dimer (marked by circles and triangles, respectively). In the last two columns, the corresponding results for the ideal, defect-free surface has been added in all panels for reference using black lines.

states, respectively.[15] Thus, on the ideal ZnO(10$\bar{1}$0) surface, only the surface O atoms are imaged at negative voltages (filled-state images), whereas only the Zn atoms are visible at positive bias (empty-state images). *F* centers, on the other hand, appear as pronounced peaks at low negative voltages because of the occupied localized defect state, which is accompanied by a strong increase in the tunneling current in the STS spectrum. This signature is found to be independent of the composition and structure of the tunneling tip. Interestingly, such pronounced peaks have been found very recently in STM experiments to be characteristic for *F* centers on MgO(001) surfaces.[7,10] However, upon increasing the voltage, an increasing number of electronic states contribute to the STM image, which starts to obscure the characteristic features of the defect state. The STM image of the O vacancy becomes very sensitive to the tip structure, in particular when positive bias voltages are applied. For the example of a tip with an O apex impurity (Figure 2e), even contrast inversion can occur compared to a clean W tip.

The thermodynamically preferred ZnO-dimer vacancy, in contrast, is always imaged as a pronounced hole, independent of the applied tunneling conditions and specific details of the tip structure. This appearance is amplified by a strong outward relaxation of the neighboring Zn ions. Simultaneously, the tunneling current in the STS spectrum above the defect decreases by at least a factor of two. The STM images of the Zn vacancy are dominated by the strong relaxation of the surface O atom next to the vacancy. The O atom is pushed out of the surface by 0.15 Å and moves 1.04 Å in the [0001] direction. Thus, a large gap is opened, which is visible for both bias polarities (independent of the tip structure). This gap is observed together with a pronounced peak from the relaxed O atom next to the vacancy, which dominates the images at certain bias voltages.

Overall, this analysis clearly shows that the various defect types yield characteristic and distinguishable STM signatures. These data change in a well-defined manner upon altering the tunneling conditions, in particular the applied bias voltage, and thus allow for an unambiguous discrimination of the different defects. In recent experimental STM studies, only very low concentrations of atomic-sized defects have been observed on the ZnO(10$\bar{1}$0) surface.[23–25] However, these defects always appear as featureless holes, whereas no pronounced peaks have been reported. Though the available experimental data is rather limited (in particular, there are no studies on the voltage dependence of the appearance of the atomic defects), these data, in conjuction with our thermodynamic calculations, suggest that the holes correspond to ZnO-dimer vacancies, while *F* centers should indeed be absent.

In conclusion, missing ZnO dimers, which are paired combinations of an *F* center and a Zn vacancy, are predicted to be the thermodynamically favored defect type on the nonpolar (10$\bar{1}$0) surface of ZnO. Calculated STM and STS data show that they are experimentally distinguishable from both *F* centers and Zn vacancies. The finding that *F* centers are basically absent has an immediate impact on the understanding of ZnO as an industrially important catalyst used for many hydrogenation and dehydrogenation reactions. The capability of ZnO to catalyze the hydrogenation of CO to form methanol[11,12] has been ascribed to *F* centers as the active sites.[26,27] However, the reaction is found to be

structure-sensitive,[28] with nonpolar ZnO surfaces such as $(10\bar{1}0)$ being less active than their polar counterparts. In light of our findings, the structure sensitivity could be elegantly explained by the strong suppression of the concentration of catalytically active *F* centers on the nonpolar ZnO$(10\bar{1}0)$ surface at the relevant experimental conditions. Thus, when studying the reactivity of oxide surfaces, the presence of *F* centers cannot be taken for granted, as it is often done in theoretical studies. Instead, for each specific case, their thermodynamic stability has to be investigated and the prevailing atomic defects at the temperature and pressure conditions of the chemical reaction of interest have to be identified.

Received: October 27, 2006
Revised: March 8, 2007
Published online: May 24, 2007

Keywords: density functional calculations · scanning probe microscopy · surface chemistry · surface defects · zinc oxide

[1] a) V. E. Henrich, P. A. Cox, *The Surface Science of Metal Oxides*, Cambridge University Press, **1994**; b) C. Noguera, *Physics and Chemistry at Oxide Surfaces*, Cambridge University Press, **1996**.
[2] G. Pacchioni, *ChemPhysChem* **2003**, *4*, 1041.
[3] I. M. Brookes, C. A. Muryn, G. Thornton, *Phys. Rev. Lett.* **2001**, *87*, 266103.
[4] R. Schaub, P. Thostrup, N. Lopez, E. Lægsaard, I. Stensgaard, J. K. Nørskov, F. Besenbacher, *Phys. Rev. Lett.* **2001**, *87*, 266104.
[5] a) S. Abbet, A. Sanchez, U. Heiz, W. D. Schneider, A. M. Ferrari, G. Pacchioni, N. Rösch, *J. Am. Chem. Soc.* **2000**, *122*, 3453; b) S. Abbet, U. Heiz, H. Häkkinen, U. Landman, *Phys. Rev. Lett.* **2001**, *86*, 5950.
[6] a) B. Yoon, H. Häkkinen, U. Landman, A. S. Wörz, J.-M. Antonietti, S. Abbet, K. Judai, U. Heiz, *Science* **2005**, *307*, 403; b) M. Arenz, U. Landman, U. Heiz, *ChemPhysChem* **2006**, *7*, 1871.
[7] M. Sterrer, E. Fischbach, T. Risse, H.-J. Freund, *Phys. Rev. Lett.* **2005**, *94*, 186101.
[8] M. R. Castell, P. L. Wincott, N. G. Condon, C. Muggelberg, G. Thornton, S. L. Dadrev, A. P. Sutton, G. A. D. Briggs, *Phys. Rev. B* **1997**, *55*, 7859.
[9] H. Nörenberg, G. A. D. Briggs, *Phys. Rev. Lett.* **1997**, *79*, 4222.
[10] M. Sterrer, M. Heyde, M. Novicki, N. Nilius, T. Risse, H.-P. Rust, G. Pacchioni, H.-J. Freund, *J. Phys. Chem. B* **2006**, *110*, 46.
[11] J. M. Thomas, W. J. Thomas, *Principles and Practice of Heterogeneous Catalysis*, VCH, Weinheim, **1997**.
[12] G. A. Olah, A. Goeppert, G. K. S. Prakash, *Beyond Oil and Gas: The Methanol Economy*, Wiley-VCH, Weinheim, **2006**.
[13] Y. Wang, B. Meyer, X. Yin, M. Kunat, D. Langenberg, F. Traeger, A. Birkner, C. Wöll, *Phys. Rev. Lett.* **2005**, *95*, 266104.
[14] a) B. Meyer, D. Marx, O. Dulub, U. Diebold, M. Kunat, D. Langenberg, C. Wöll, *Angew. Chem.* **2004**, *116*, 6809; *Angew. Chem. Int. Ed.* **2004**, *43*, 6641; b) O. Dulub, B. Meyer, U. Diebold, *Phys. Rev. Lett.* **2005**, *95*, 136101.
[15] B. Meyer, D. Marx, *Phys. Rev. B* **2003**, *67*, 035403.
[16] C. G. Van de Walle, D. B. Laks, G. F. Neumark, S. T. Pantelides, *Phys. Rev. B* **1993**, *47*, 9425.
[17] G.-X. Qian, R. M. Martin, D. J. Chadi, *Phys. Rev. B* **1988**, *38*, 7649.
[18] B. Meyer, *Phys. Rev. B* **2004**, *69*, 045416.
[19] a) J. Hutter et al., see: http://www.cpmd.org; b) "Ab Initio Molecular Dynamics: Theory and Implementation": D. Marx, J. Hutter in *Modern Methods and Algorithms of Quantum Chemistry* (Ed.: J. Grotendorst), NIC, FZ Jülich, **2000**, see http://www.theochem.rub.de/go/cprev.html.
[20] K. Johnston, M. R. Castell, A. T. Paxton, M. W. Finnis, *Phys. Rev. B* **2004**, *70*, 085415.
[21] W. A. Hofer, A. S. Foster, A. L. Shluger, *Rev. Mod. Phys.* **2003**, *75*, 1287.
[22] In the STM/STS calculations, the ultrasoft pseudopotentials were replaced by norm-conserving ones, and the plane-wave cut-off energy was increased to 120 Ry in order to obtain smooth wave function tails in the vacuum region.
[23] T. M. Parker, N. G. Cordon, R. Lindsay, F. M. Leibsle, G. Thornton, *Surf. Sci.* **1998**, *415*, L1046.
[24] a) O. Dulub, L. A. Boatner, U. Diebold, *Surf. Sci.* **2002**, *519*, 201; b) U. Diebold, L. Vogel-Koplitz, O. Dulub, *Appl. Surf. Sci.* **2004**, *237*, 336.
[25] X.-L. Yin, A. Birkner, K. Hänel, T. Löber, U. Köhler, C. Wöll, *Phys. Chem. Chem. Phys.* **2006**, *8*, 1477.
[26] S. A. French, A. A. Sokol, S. T. Bromlely, C. R. A. Catlow, S. C. Rogers, F. King, P. Sherwood, *Angew. Chem.* **2001**, *113*, 4569; *Angew. Chem. Int. Ed.* **2001**, *40*, 4437.
[27] M. Kurtz, J. Strunk, O. Hinrichsen, M. Muhler, K. Fink, B. Meyer, C. Wöll, *Angew. Chem.* **2005**, *117*, 2850; *Angew. Chem. Int. Ed.* **2005**, *44*, 2790.
[28] H. Wilmer, M. Kurtz, K. V. Klementiev, O. P. Tkachenko, W. Grünert, O. Hinrichsen, A. Birkner, S. Rabe, K. Merz, M. Driess, C. Wöll, M. Muhler, *Phys. Chem. Chem. Phys.* **2003**, *5*, 4736.

